Charmonium chemistry in $A+A$ collisions at relativistic energies

E. L. Bratkovskaya,[1] A. P. Kostyuk,[1,2] W. Cassing,[3] and H. Stöcker[1]
[1]*Institut für Theoretische Physik, Universität Frankfurt, 60054 Frankfurt, Germany*
[2]*Bogolyubov Institute for Theoretical Physics, 03143 Kyiv, Ukraine*
[3]*Institut für Theoretische Physik, Universität Giessen, 35392 Giessen, Germany*
(Received 12 February 2004; published 26 May 2004)

Charmonium production and suppression in heavy-ion collisions at relativistic energies is investigated within different models, i.e., the comover absorption model, the threshold model, the statistical coalescence model, and the hadron-string-dynamics (HSD) transport approach. In HSD the charmonium dissociation cross sections with mesons are described by a simple phase-space parametrization including an effective coupling strength $|M_i|^2$ for the charmonium states $i=\chi_c, J/\psi, \psi'$. This allows inclusion of the backward channels for charmonium reproduction by $D\bar{D}$ channels—which are missed in the comover absorption and threshold model—employing detailed balance without introducing any new parameters. It is found that all approaches yield a reasonable description of J/ψ suppression in S+U and Pb+Pb collisions at Super Proton Synchrotron (SPS) energies. However, they differ significantly in the $\psi'/J/\psi$ ratio versus centrality at SPS and especially at Relativistic Heavy-Ion Collider (RHIC) energies. These pronounced differences can be exploited in future measurements at RHIC to distinguish the hadronic rescattering scenarios from quark coalescence close to the quark-gluon plasma phase boundary.

DOI: 10.1103/PhysRevC.69.054903 PACS number(s): 25.75.−q, 13.60.Le, 14.40.Lb, 14.65.Dw

I. INTRODUCTION

The dynamics of ultrarelativistic nucleus-nucleus collisions at Super Proton Synchrotron (SPS) and Relativistic Heavy-Ion Collider (RHIC) energies are of fundamental interest with respect to the properties of hadronic/partonic systems at high energy densities. In particular, the formation of a quark-gluon plasma (QGP) and its transition to interacting hadronic matter has motivated a large community for more than two decades [1–4]. However, the complexity of the dynamics has not been unraveled and the evidence for the formation of a QGP and/or the properties of the phase transition is much debated [5]. Apart from the light and strange flavor $(u,\bar{u},d,\bar{d},s,\bar{s})$ quark physics and their hadronic bound states in the vacuum $(p,n,\pi,K,\phi,\Lambda$, etc.), the interest in hadrons with charm $(c,\bar{c})$ has been rising continuously since the heavy charm quark provides an additional energy scale, which is large compared to Λ_{QCD}. The $c,\bar{c}$ quark degrees of freedom are of particular interest in the context of the phase transition to the QGP since $c\bar{c}$ meson states might no longer be formed due to color screening [6,7].

However, the suppression of J/ψ and ψ' mesons in the high density phase of nucleus-nucleus collisions at SPS energies [8–13] might also be attributed to a large extent to inelastic comover scattering (cf. [3,14–20] and references therein) provided that the corresponding J/ψ-hadron cross sections are of the order of a few millibarns [20–25]. Theoretical estimates here differ by more than an order of magnitude (cf. [25–28] and references therein), especially with respect to J/ψ-meson scattering, such that the question of charmonium suppression is not yet settled. On the other hand, at RHIC energies further absorption mechanisms—such as plasma screening and gluon scattering—might play a dominant role as suggested in Refs. [29,30] and also lead to a substantial reduction of the J/ψ formation in central Au+Au collisions.

Furthermore, it has been pointed out—within statistical models—that at RHIC energies the charmonium formation from open charm and anticharm mesons might become essential [31–34] and even exceed the yield from primary NN collisions [35]. One of the prevailing questions is thus if open charm mesons and charmonia will achieve thermal equilibrium with the light mesons during the nucleus-nucleus reaction. Furthermore, does the distribution of charm (anti)-quarks over open and hidden charm mesons conform with the statistical law at the same freeze-out parameters as anticipated in Refs. [31–34]?

In fact, a previous analysis within the hadron-string-dynamics (HSD) transport model [36] has demonstrated that the charmonium production from open charm and anticharm mesons becomes essential in central Au+Au collisions at the RHIC. This is in accordance with independent studies in Refs. [23,30]. On the other hand, these backward channels have been found to be practically negligible at SPS energies. There is, however, an experimental claim [37] that open charm might be enhanced by up to a factor of 3 in central nucleus-nucleus collisions. In this case the hidden charm regeneration processes might already be essential in (semi)central collisions at SPS energies [32–34]. A possible reason for the open charm enhancement is an increase of the effective production cross sections of heavy quarks in the strongly interacting medium [38]. Also strong secondary meson-baryon channels might be responsible for this enhancement as pointed out in Ref. [39]. In short, there are presently more open questions than solid answers.

Here we extend our previous studies [36] with respect to observable ratios of charmonium states, i.e., in particular the $\psi'/J/\psi$ ratio, which is accessible by experiment. We compare the HSD results to the calculations within the standard scenarios (including only suppression channels) as well as within the statistical coalescence model (SCM) [31].

Our work is organized as follows. In Sec. II we remind the reader of the standard models of charmonium suppression as well as of the statistical coalescence model. We also briefly recall the "input" of the HSD transport approach with respect to charmonium and open charm degrees of freedom. In Sec. III the results of all models are presented for S+U collisions at $\sqrt{s}=20$ GeV, for Pb+Pb collisions at $\sqrt{s}=17.3$ GeV, and Au+Au collisions at $\sqrt{s}=200$ GeV. We present the yields of J/ψ and ψ' as well as their ratio as a function of centrality. Section IV gives a summary of our findings.

II. DESCRIPTION OF THE MODELS

A. The standard models

The standard approach to charmonium production in heavy-ion collisions assumes that $c\bar{c}$ bound states are created *only* at the initial stage of the reaction in primary nucleon-nucleon collisions. During the subsequent evolution of the system, the number of hidden charm mesons is *suppressed* by (i) the absorption of preresonance charmonium states in nuclei (the normal nuclear suppression), (ii) the interactions of charmonia with secondary hadrons (comovers), and (iii) a possible dissociation of $c\bar{c}$ bound states in the deconfined medium. The last mechanism was first expected in Ref. [6] and it was proposed that charmonia might be used as a probe for deconfinement in the state of matter created at the early stage of the collision.

Two basic versions of the standard scenarios have been considered in the literature that are both restricted to suppression mechanisms only. One of them, the comover model [14], assumes that the charmonium increases gradually with the density of the strongly interacting medium created in the collision. No abrupt changes of absorption properties of the medium take place. The model of Ref. [40] represents the opposite extreme: the suppression sets in abruptly as soon as the energy density exceeds a threshold value, which is a free parameter of this model. This version of the "suppression-only" approach will be referred to as "the threshold scenario." The latter model is motivated by the idea that the charmonium dissociation rate is drastically higher in a quark-gluon plasma than in a hadronic medium.

For a brief description of the "suppression-only" approach let us consider two nuclei A and B that collide at impact parameter b. The number of produced hidden charm mesons is given by [41]

$$N_i^{AB}(b) = \sigma_i^{NN} AB \int d^2s\; T_A(|\vec{s}|) T_B(|\vec{s}-\vec{b}|) S(\vec{b},\vec{s}), \qquad (1)$$

where σ_i^{NN} is the production cross section of the charmonium species i in nucleon-nucleon $(N+N)$ collisions, $T_{A(B)}$ is the nuclear thickness function related to the nucleon density in the nucleus, and $S(\vec{b},\vec{s})<1$ is a factor responsible for the charmonium suppression.

At the very initial stage charmonia experience absorption, $S=S^{abs}$, by interactions with nucleons of the colliding nuclei (see, for instance, Refs. [14,41]). Bound $c\bar{c}$ states are assumed to be absorbed in the so-called "preresonance state" before the final hidden charm mesons are formed. This absorption cross section is therefore taken to be the same for all charmonia. The cross section $\sigma_{abs}=4.4$ mb [42] is taken from the most recent SPS data analysis and is close to the theoretical prediction of Ref. [43]. We assume that the same cross section σ_{abs} prevails also at RHIC energies.

Those charmonia—that survive normal nuclear suppression—are furthermore subjected to the comover [3,14–20] or quark-gluon plasma suppression [40]. We recall that both scenarios describe successfully the centrality dependence of the J/ψ yield in Pb+Pb collisions at the SPS. In the comover approach, an additional factor appears: $S=S^{abs}S^{co}$ [14], which depends on the density of comovers and on an *effective* cross section σ_{co} for charmonium dissociation by comovers. The value $\sigma_{co}^{J/\psi}=1.0$ mb is obtained from the fit of the NA50 data on J/ψ production in Pb+Pb at the SPS (new data [12] were added). It also agrees with the NA38 data for S+U collisions. This value corresponds to an average over all comover species, relative collision energies as well as all charmonium states contributing to the J/ψ yield through their decays. From a fit of the ψ' to J/ψ ratio in S+U collisions at SPS we get the value $\sigma_{co}^{\psi'}=5$ mb for the effective cross section of ψ' suppression. We will assume that the cross sections $\sigma_{co}^{J/\psi,\psi'}$ are the same also at the RHIC energies; however, the charmonium suppression at the RHIC becomes stronger due to the higher comover density.

There are two reasons for an increased comover density at the RHIC relative to the SPS. (a) The multiplicity of produced secondary hadrons per unit rapidity interval at midrapidity already increases by a factor of about 1.5 from $\sqrt{s}=17$ GeV to $\sqrt{s}=200$ GeV in elementary nucleon-nucleon collisions; (b) the deviations from the wounded nucleon model become stronger at higher energies, which increases the comover density in central nucleus-nucleus collisions additionally. The centrality dependence of the number of light-flavored hadrons per unit pseudorapidity interval in Au+Au collisions at the RHIC can be parametrized as [44]

$$\left.\frac{dN_h^{\mathrm{AuAu}}}{dy}\right|_{y=0} = \left.\frac{dN_h^{pp}}{dy}\right|_{y=0} [(1-x)N_p/2 + xN_{coll}], \qquad (2)$$

where $x=0.11$ for $\sqrt{s}=200$ GeV [45], $N_p(b)$ is the number of participants, and $N_{coll}(b)$ is the number of collisions. Both are evaluated in the Glauber approach.

Calculating the centrality dependence of the charmonium suppression, it is convenient to introduce an *reactant* density in the plane transverse to the collision axis:

$$n_p^*(\vec{b},\vec{s}) = [(1-x)n_p(\vec{b},\vec{s}) + 2xn_c(\vec{b},\vec{s})]. \qquad (3)$$

Here $n_p(\vec{b},\vec{s})$ and $n_c(\vec{b},\vec{s})$ are, respectively, the densities of nucleon participants and collisions in the transverse plane:

$$N_p(b) = \int d^2s\; n_p(\vec{b},\vec{s}) \qquad (4)$$

and

$$N_{coll}(b) = \int d^2s\, n_{coll}(\vec{b},\vec{s}). \quad (5)$$

Note that the multiplicity of light-flavored hadrons (2) is proportional to

$$N_p^*(b) = \int d^2s\, n_p^*(\vec{b},\vec{s}). \quad (6)$$

Motivated by this fact, we assume that the comover *density* in the transverse plane, which is needed to calculate S^{co}, is proportional to n_p^* (3).

In contrast to the comover version of the models, the threshold scenario [40] assumes that no charmonia are destroyed by the medium until the energy density reaches a threshold value. The excited charmonia χ_c, which contribute about 40% to the total J/ψ yield, are suppressed at lower energy densities compared to directly produced J/ψ's. We have updated the fit [46] to the SPS data (new NA50 data [12] were added) using the corrected value of the normal nuclear absorption cross section $\sigma_{abs}=4.4\pm0.5$ mb [47]. The J/ψ to Drell-Yan ratio in nucleon-nucleon collisions is aproximately the same as in Ref. [46]: $\sigma_{J/\psi}^{NN}/\sigma_{DY}^{NN}\approx 53$. Our results are[1] $n_\chi=2.0$ fm^{-2} and $n_{J/\psi}=3.8$ fm^{-2}. Here n_χ ($n_{J/\psi}$) is the participant density in the transverse plane corresponding to the threshold energy density at which χ_c charmonia (J/ψ's) are fully suppressed. (The change of the J/ψ yield due to the ψ' is neglected.) The threshold for the ψ' suppression $n_{\psi'}=1.7$ is obtained from a fit of the ψ' to J/ψ ratio in S+U collisions at the SPS.

Extrapolating to RHIC energies, one again has to take into account that the number of produced hadrons per unit rapidity and, consequently, the energy density of the produced medium grows with the collision energy and centrality. Due to deviations from the wounded nucleon model (2) the charmonium suppression sets in when the *effective* participant density $n_p^*(\vec{b},\vec{s})$ (3)—rather than $n_p(\vec{b},\vec{s})$—exceeds the threshold value. The number of secondary hadrons per *effective* participant pair at $\sqrt{s}=200$ is higher than that at the SPS by a factor of about 1.5. The critical energy density at the RHIC is reached, therefore, at lower effective participant density: $n_\chi^*=n_\chi/1.5\approx 1.3$ fm^{-2}, $n_{J/\psi}^*=n_{J/\psi}/1.5\approx 2.5$ fm^{-2}, and $n_{\psi'}^*=n_{\psi'}/1.5\approx 1.1$ fm^{-2}.

B. Statistical coalescence model

In contrast to the scenario described in Sec. II A, the statistical coalescence model [31] assumes that hidden and open charm hadrons are created at hadronization near the point of chemical freeze-out, which might be close to the phase boundary of the QGP. However, contrary to the pure thermal model [49] the total amount of charm in the system is not assumed to be in chemical equilibrium. Indeed the relaxation time for the number of c and $\bar{c}$ is expected to exceed the lifetime of the system. Therefore, the total charm content of the final hadron system is assumed to be equal to the number of c and $\bar{c}$ created at the initial stage of $A+A$ reactions by nucleon-nucleon collisions. Only the distribution of c and $\bar{c}$ among different hadron states is controlled by statistical laws in terms of the hadron gas (HG) model parameters: i.e., temperature T, baryonic chemical potential μ_B, and volume V. It appears that the number of hidden charm mesons produced by a statistical coalescence mechanism depends weakly on the thermodynamic hadronization parameters T and μ_B. The charmonium yield is mainly defined by the average number of charmed quark-antiquark pairs $\overline{N}_{c\bar{c}}$ and by the hadronization volume parameter V. We recall that, if $\overline{N}_{c\bar{c}}$ is not much larger than unity, a proper account for the exact charm conservation becomes essential as shown in Ref. [32]. This is crucial at SPS energies, where $\overline{N}_{c\bar{c}}$ is less than unity, and remains essential for moderate centralities in Au+Au collisions at the RHIC.

The SCM formula for the *total* (4π) charmonium yield, that takes into account exact conservation of the number of $c\bar{c}$ pairs, was obtained in Ref. [32]. In the real experimental situation, however, measurements are performed in a limited rapidity window Δy. In the most simple case, when the fraction of charmonia in the relevant rapidity window does not depend on the centrality, one can merely use the formula for the total yield multiplied by some factor $\xi<1$. This approach was used in Refs. [33,34] for studying the SPS data, where the multiplicity of light hadrons, which determine the freeze-out volume of the system, are approximately proportional to the number of nucleon participants N_p at all rapidities. At the RHIC the situation is different: the *total* (4π) multiplicity of light hadrons is approximately proportional to the number of participants N_{part}, while *at midrapidity* it grows faster with N_{part} [see Eq. (2)]. The centrality dependence of charmonium production at different rapidities should, in this case, be also different. To compare the SCM prediction to the PHENIX data [50], which are related to the J/ψ yield at midrapidity $dN_{J/\psi}/dy$, one has to derive a formula for the charmonium yield in a *finite* rapidity interval Δy.

To this aim let $\xi_{\Delta y}<1$ be the probability that a c quark, produced in a nucleus-nucleus collision, has rapidity y within the interval Δy. The probability distribution of the number k_c of c quarks inside the interval Δy for events with fixed *total* (4π) number $N_{c\bar{c}}$ of $c\bar{c}$ pairs is given by the binomial law:

$$f(k_c|N_{c\bar{c}}) = \frac{N_{c\bar{c}}!}{k_c!\,(N_{c\bar{c}}-k_c)!}\,\xi_{\Delta y}^{k_c}(1-\xi_{\Delta y})^{N_{c\bar{c}}-k_c}. \quad (7)$$

The probability distribution of the number $k_{\bar{c}}$ of $\bar{c}$'s inside the interval Δy is assumed to be *independent* of k_c.[2] It conforms to the same binomial law. Event-by-event fluctuations of the number of $c\bar{c}$ pairs $N_{c\bar{c}}$, created at the early stage of $A+A$ reactions in independent nucleon-nucleon collisions are Poisson distributed:

[1] These numbers are different from those of Ref. [48], where another value of the J/ψ to Drell-Yan ratio in nucleon-nucleon collisions $\sigma_{J/\psi}^{NN}/\sigma_{DY}^{NN}\approx 43$ was assumed.

[2] This differs from Ref. [51], where an exact equality, $k_c=k_{\bar{c}}$, within the chosen interval Δy is assumed. In fact, the net charm is exactly zero only in the total system. In any finite rapidity interval, however, event-by-event fluctuations with $k_c\neq k_{\bar{c}}$ are possible.

$$P(N_{c\bar{c}};\overline{N}_{c\bar{c}}) = \exp(-\overline{N}_{c\bar{c}})\,\frac{(\overline{N}_{c\bar{c}})^{N_{c\bar{c}}}}{N_{c\bar{c}}!}. \tag{8}$$

The probability of $c\bar{c}$ coalescence is proportional to the product of their numbers and inversely proportional to the system volume. The proportionality coefficient depends on the thermal densities of the open and hidden charm hadrons, and is the same as in the case of the total charmonium yield [32].

The average multiplicity of the charmonium species i at fixed values of k_c and $k_{\bar{c}}$ is therefore given by [52]

$$N_i^{\Delta y}(k_c k_{\bar{c}}) \approx k_c k_{\bar{c}} \frac{n_i^{tot}}{(n_O/2)^2}\,\frac{1}{V_{\Delta y}}. \tag{9}$$

In deriving Eq. (9) we used the fact that the thermal number of hadrons with hidden charm is much smaller than that with open charm. Folding Eq. (9) with the binomial and Poisson distributions one gets

$$N_i^{\Delta y} \approx \xi_{\Delta y}^2\,\overline{N}_{c\bar{c}}(\overline{N}_{c\bar{c}}+1)\,\frac{n_i^{tot}}{(n_O/2)^2}\,\frac{1}{V_{\Delta y}}, \tag{10}$$

where n_O is the thermal density of all open charm hadrons and n_i^{tot} is the total thermal density of the charmonium species i (including the decay contributions from the higher charmonium states). Both n_O and n_i^{tot} are calculated in the grand-canonical ensemble with the QGP hadronization parameters $T, \mu_B, V_{\Delta y}$ found from fitting the data of light-flavored[3] hadron yields in the rapidity interval Δy. The average number of $c\bar{c}$ pairs $\overline{N}_{c\bar{c}}$ is, however, related to their *total* (4π) yield.

The distinctive feature of the statistical coalescence model is that the *ratio* of multiplicities of different charmonium species is the same as in the equlibrium hadron gas. Therefore the ψ' to J/ψ ratio is practically independent on the centrality and only slightly depends on the collision energy (due to the change of freeze-out parameters).

In Au+Au collisions at $\sqrt{s}=200$ GeV the yield of light-flavored hadrons at midrapidity is fitted within the hadron gas model with $T=177$ MeV and $\mu_B=29$ MeV [53]. The centrality dependence of the volume is calculated from

$$V_{\Delta y=1} = \frac{1}{n_{ch}(T,\mu_B)}\,1.2\,\frac{dN_{ch}^{\mathrm{AuAu}}}{d\eta}; \tag{11}$$

the coefficient 1.2 is needed to recalculate the number of particles per unit *pseudorapidity* (η) interval to that per unit *rapidity* (y) interval [54]. Here n_{ch} is the charged hadron density calculated in the HG model.

The average number of the initially produced $c\bar{c}$ pairs in our calculations is proportional to the number of binary nucleon-nucleon collisions:

$$\overline{N}_{c\bar{c}} = N_{coll}(b)\;\sigma_{c\bar{c}}^{NN}/\sigma_{inel}^{NN}. \tag{12}$$

Our statistical coalescence model calculations are performed under the assumption that the open charm multiplicity is enhanced in nucleus-nucleus collisions at the SPS according to the experimental claim in Ref. [37]; therefore the effective charm production cross section $\sigma_{c\bar{c}}^{NN}$ in Eq. (12) is assumed to be larger by a factor of ~ 3.5 than in elementary nucleon-nucleon collisions. This "enhancement" factor is expected to become weaker at larger collision energies [38]. Therefore, we neglect it in our calculations for the RHIC.

The charm production cross section $\sigma_{c\bar{c}}^{NN}$ has been measured at the RHIC by the PHENIX Collaboration [55]. The result is consistent with PYTHIA calculations: $\sigma_{c\bar{c}}^{NN} \approx 650\ \mu$b. This gives $\overline{N}_{c\bar{c}} \approx 16-17$ for central Au+Au collisions in line with the HSD calculations in Ref. [56].

The SCM is applicable only to large systems: $N_{part} > 100$ in Pb+Pb at the SPS [31,33,34]. Therefore, the PHENIX's $p+p$ point and the most peripheral Au+Au point, corresponding to $N_{part} \approx 30$, cannot be used in the SCM fit procedure. For this reason we restrict ourselves only to a rough estimate of the SCM prediction for the charmonium yield at midrapidity at the top RHIC energy.

We fix the charm production cross section in nucleon-nucleon collisions at its PYTHIA value, $\sigma_{c\bar{c}}^{NN}=650\ \mu$b. Since there are no experimental data for the value of $\xi_{\Delta y=1}$, one can roughly estimate it assuming approximately the same rapidity distribution for the open charm and J/ψ's in $p+p$ collisions. This leads to $\xi_{\Delta y=1} \approx 0.3$. We note that the charm rapidity distribution in Au+Au collisions might be broader than in $p+p$ reactions due to rescattering of c and $\bar{c}$ with nucleons. This will not change our result essentially, however. The estimate of the total charm production cross section is based on the single electron measurement at midrapidity. Any extrapolation to the total phase space has been done assuming that the charm rapidity distribution does not change from $p+p$ to Au+Au. The charm production rate per binary collision at midrapidity was found to be independent of the centrality (at least within the present accuracy of the measurement). This implies that the total charm production cross section should grow with the centrality, if there is a broadening of the rapidity distribution. Both effects, the decrease of $\xi_{\Delta y=1}$ and the increase of $\sigma_{c\bar{c}}^{NN}$ nearly cancel each other in Eq. (10) such that the prediction of SCM does not change significantly.

C. Open charm and charmonium dynamics in HSD

In order to examine the dynamics of open charm and charmonium degrees of freedom during the formation and expansion phase of the highly excited system created in a relativistic nucleus-nucleus collision within transport approaches, one has to know the number of initially produced particles with c or $\bar{c}$ quarks, i.e., $D, \bar{D}, D^*, \bar{D}^*$, $D_s, \bar{D}_s, D_s^*, \bar{D}_s^*, J/\psi(1S), \psi'(2S), \chi_c(1P)$. In this work we follow the previous studies in Refs. [3,17,36,56] and fit the total charmonium production cross sections $(i=\chi_c, J/\psi, \psi')$ from

[3] At the RHIC the strangeness as well as all other conserved charges, excluding charm, can be safely considered in the grand canonical ensemble.

NN collisions as a function of the invariant energy $\sqrt{s}$ by the function

$$\sigma_i^{NN}(s) = f_i\, a\left(1-\frac{m_i}{\sqrt{s}}\right)^{\alpha}\left(\frac{\sqrt{s}}{m_i}\right)^{\beta}\theta(\sqrt{s}-\sqrt{s_{0i}}), \qquad (13)$$

where m_i denotes the mass of charmonium i while $\sqrt{s_{0i}}=m_i+2m_N$ is the threshold in vacuum. The parameters in (13) have been fixed to describe the J/ψ and ψ' data at lower energy ($\sqrt{s}\leqslant 30$ GeV) as well as the data point from the PHENIX Collaboration [57] at $\sqrt{s}=200$ GeV, which gives $\sigma(pp\rightarrow J/\psi+X)=3.99\pm0.61(\text{stat})\pm0.58[\text{syst}\pm0.40(\text{abs})]$ μb for the total J/ψ cross section. We use $a=0.2$ mb, $\alpha=10$, $\beta=0.775$. The parameters f_i are the fractions of charmonium states i. For the present study we choose $f_{\chi_c}=0.636$, $f_{J/\psi}=0.581$, $f_{\psi'}=0.21$ in order to reproduce the experimental ratio

$$\frac{B(\chi_{c1}\rightarrow J/\psi)\sigma_{\chi_{c1}}+B(\chi_{c2}\rightarrow J/\psi)\sigma_{\chi_{c2}}}{\sigma_{J/\psi}^{expt}}=0.344\pm0.031$$

measured in pp and πN reactions [58,59] as well as the averaged pp and pA ratio

$$[B_{\mu\mu}(\psi')\sigma_{\psi'}]/[B_{\mu\mu}(J/\psi)\sigma_{J/\psi}]\simeq 0.0165$$

(cf. the compilation of experimental data in Ref. [47]). Here the experimentally measured J/ψ cross section includes the direct J/ψ component ($\sigma_{J/\psi}$) as well as the decays of higher charmonium states χ_c, ψ', i.e.,

$$\sigma_{J/\psi}^{expt}=\sigma_{J/\psi}+B(\chi_c\rightarrow J/\psi)\sigma_{\chi_c}+B(\psi'\rightarrow J/\psi)\sigma_{\psi'}. \qquad (14)$$

Note, we do not distinguish here the $\chi_{c1}(1P)$ and $\chi_{c2}(1P)$ states. Instead, we use only the $\chi_{c1}(1P)$ state (which we denote as χ_c); however, with an increased branching ratio for the decay to J/ψ in order to include the contribution of $\chi_{c2}(1P)$, i.e., $B(\chi_c\rightarrow J/\psi)=0.54$. We adopt $B(\psi'\rightarrow J/\psi)=0.557$ from [60].

For the total charmonium production cross sections from πN reactions we use the parametrization (in line with Ref. [15]):

$$\sigma_i^{\pi N}(s)=f_i\; b\left(1-\frac{m_i}{\sqrt{s}}\right)^{\gamma}\theta(\sqrt{s}-\sqrt{s_{0i}}), \qquad (15)$$

with $\gamma=7.3$ and $b=1.24$ mb, which describes the existing experimental data at low $\sqrt{s}$ reasonably well (cf. Fig. 3 from [56]). $\sqrt{s_{0i}}=m_i+m_N+m_\pi$ is the threshold in vacuum for πN reactions.

Apart from the total cross sections, we also need the differential distribution of the produced mesons in the transverse momentum p_T and the rapidity y (or Feynman x_F) from each individual collision. We recall that $x_F=p_z/p_z^{max}\approx 2p_z/\sqrt{s}$ with p_z denoting the longitudinal momentum. For the differential distribution in x_F from NN and πN collisions we use the ansatz from the E672/E706 Collaboration [61]:

$$\frac{dN}{dx_F dp_T}\sim(1-|x_F|)^c\exp(-b_{p_T}p_T), \qquad (16)$$

where $b_{p_T}=2.08$ GeV^{-1} and $c=a/(1+b/\sqrt{s})$. The parameters a, b are chosen as $a_{NN}=13.5$, $b_{NN}=24.9$ for NN collisions and $a_{\pi N}=4.11$, $b_{\pi N}=10.2$ for πN collisions as in [36,56].

The total and differential cross sections for open charm mesons from pp collisions, furthermore, are taken as in Refs. [36,56]. We thus refer to the results of Ref. [56] which give ~ 16 $D\bar{D}$ pairs in central Au+Au collisions at $\sqrt{s}=200$ GeV, a factor of ~ 160 relative to the expected primordial J/ψ multiplicity.

Apart from primary hard NN collisions the open charm mesons or charmonia may also be generated by secondary meson-baryon (mB) reactions. Here we include all secondary collisions of mesons with baryons by assuming that the open charm cross section (from Sec. 2 of Ref. [56]) depends only on the invariant energy $\sqrt{s}$ and not on the explicit meson or baryon state. Furthermore, we take into account all interactions of "formed" mesons—after a formation time of $\tau_F=0.8$ fm/c (in their rest frame) [62]—with baryons or diquarks, respectively. As pointed out in Ref. [56] the production of open charm pairs in central Au+Au collisions by mB reactions at RHIC energies is expected to be on the 10% level.

In order to study the effect of rescattering we tentatively adopt the following dissociation cross sections of charmonia with baryons independent on the energy (in line with Refs. [17,56]):

$$\sigma_{c\bar{c}B}=6\text{ mb}, \qquad (17)$$

$$\sigma_{J/\psi B}=4\text{ mb},\ \sigma_{\chi_c B}=5\text{ mb},\ \sigma_{\psi' B}=5\text{ mb}.$$

In Eqs. (17) the cross section $\sigma_{c\bar{c}B}$ stands for a (color dipole) preresonance ($c\bar{c}$)–baryon cross section, since the $c\bar{c}$ pair produced initially cannot be identified with a particular hadron due to the uncertainty relation in energy and time. For the lifetime of the preresonance $c\bar{c}$ pair (in its rest frame) a value of $\tau_{c\bar{c}}=0.3$ fm/c is assumed following Ref. [63]. This value corresponds to the mass difference of the ψ' and J/ψ.

For D, D^*, $\bar{D}$, $\bar{D}^*$–meson (π,η,ρ,ω) scattering we address the calculations from Refs. [22,23] which predict elastic cross sections in the range of 10–20 mb depending on the size of the form factor employed. As a guideline we use a constant cross section of 10 mb for elastic scattering with mesons and also baryons, although the latter might be even higher for very low relative momenta.

As already pointed out in the Introduction the J/ψ formation cross sections by open charm mesons or the inverse comover dissociation cross sections are not well known and the significance of these channels is discussed controversely in the literature [26,27,31,35,64,65]. We here follow the concept of Ref. [36] and introduce a simple two-body transition model with a single parameter M_i^2 for each charmonium, that allows us to implement the backward reactions uniquely by employing detailed balance for each individual channel. Since the meson-meson dissociation and backward reactions

typically occur with low relative momenta ("comovers") it is legitimate to write the cross section for the process $1+2 \rightarrow 3+4$ as

$$\sigma_{1+2\rightarrow 3+4}(s) = 2^4 \frac{E_1E_2E_3E_4}{s} |\tilde{M}_i|^2 \left(\frac{m_3+m_4}{\sqrt{s}}\right)^6 \frac{p_f}{p_i}, \quad (18)$$

where E_k and S_k denote the energy and spin of hadron k ($k=1,2,3,4$), respectively. The initial and final momenta for fixed invariant energy $\sqrt{s}$ are given by

$$p_i^2 = \frac{[s-(m_1+m_2)^2][s-(m_1-m_2)^2]}{4s},$$

$$p_f^2 = \frac{[s-(m_3+m_4)^2][s-(m_3-m_4)^2]}{4s}, \quad (19)$$

where m_k denotes the mass of hadron k. In Eq. (18) $|\tilde{M}_i|^2$ ($i=\chi_c, J/\psi, \psi'$) stands for the effective matrix element squared which for the different two-body channels is taken of the form

$$|\tilde{M}_i|^2 = |M_i|^2 \text{ for } (\pi,\rho) + (c\bar{c})_i \rightarrow D + \bar{D}, \quad (20)$$

$$|\tilde{M}_i|^2 = 3|M_i|^2 \text{ for } (\pi,\rho) + (c\bar{c})_i \rightarrow D^* + \bar{D},$$

$$D + \bar{D}^*,\ D^* + \bar{D}^*,$$

$$|\tilde{M}_i|^2 = \frac{1}{3}|M_i|^2 \text{ for } (K,K^*) + (c\bar{c})_i \rightarrow D_s + \bar{D},$$

$$\bar{D}_s + D,$$

$$|\tilde{M}_i|^2 = |M_i|^2 \text{ for } (K,K^*) + (c\bar{c})_i \rightarrow D_s + \bar{D}^*,$$

$$\bar{D}_s + D^*,\ D_s^* + \bar{D},\ \bar{D}_s^* + D,\ \bar{D}_s^* + D^*.$$

The relative factors of 3 in Eqs. (20) are guided by the sum rule studies in [28], which suggest that the cross section is increased whenever a vector meson D^* or $\bar{D}^*$ appears in the final channel while another factor of $1/3$ is introduced for each s or $\bar{s}$ quark involved. The factor $[(m_3+m_4)/\sqrt{s}]^6$ in Eq. (18) accounts for the suppression of binary channels with increasing $\sqrt{s}$ and has been fitted to the experimental data for the reactions $\pi+N\rightarrow\rho+N, \omega+N, \Phi+N, K^++\Lambda$ in Ref. [39].

In Ref. [36] we have used (for simplicity) the same matrix elements for the dissociation of all charmonium states i ($i=\chi_c, J/\psi, \psi'$) with mesons. However, there is no fundamental reason why these matrix elements should be identical. In the present study we will explore the charmonium "chemistry" explicitly and consider two different scenarios: set 1, the same matrix element for all charmonium states i as in Ref. [36]; and set 2, the matrix element squared for ψ' is enhanced by a factor of 1.5 relative to J/ψ:

$$\text{set 1: } |M_{J/\psi}|^2 = |M_{\chi_c}|^2 = |M_{\psi'}|^2 = |M_0|^2, \quad (21)$$

$$\text{set 2: } |M_{J/\psi}|^2 = |M_{\chi_c}|^2 = |M_0|^2,\ |M_{\psi'}|^2 = 1.5|M_0|^2.$$

We have fixed the parameter $|M_0|^2$ by comparison with the J/ψ suppression data from the NA38 and NA50 Collaborations for S+U and Pb+Pb collisions at 200 and 160 A GeV, respectively [10,11,13] (cf. Fig. 1 in Sec. III). We obtain the best fit for $|M_0|^2=0.17$ fm/GeV^2 (which is slightly higher than in our previous study [36] since the fractions of charmonium states f_i have been also modified here).

The advantage of the model introduced in Eq. (18) is that detailed balance for the binary reactions can be employed strictly for each individual channel, i.e.,

$$\sigma_{3+4\rightarrow 1+2}(s) = \sigma_{1+2\rightarrow 3+4}(s) \frac{(2S_1+1)(2S_2+1)}{(2S_3+1)(2S_4+1)} \frac{p_i^2}{p_f^2}, \quad (22)$$

and the role of the backward reactions [$(c\bar{c})_i$+meson formation by $D+\bar{D}$ flavor exchange] can be explored without introducing any additional parameter once $|M_i|^2$ is fixed. The uncertainty in the cross sections (18) is of the same order of magnitude as that in Lagrangian approaches using, e.g., $SU(4)_{flavor}$ symmetry [22,23] since the form factors at the vertices are essentially unknown [28]. It should be pointed out that the comover dissociation channels for charmonia are described in HSD with the proper individual thresholds for each channel in contrast to the comover absorption model described in Sec. II A.

We recall that (as in Refs. [36,56,66–68]) the charm degrees of freedom are treated perturbatively and that initial hard processes (such as $c\bar{c}$ or Drell-Yan production from NN collisions) are "precalculated" to achieve a scaling of the inclusive cross section with the number of projectile and target nucleons as $A_P \times A_T$ when integrating over impact parameter b.

We typically perform 20 parallel runs for each impact parameter b in steps of $\Delta b=0.5$ fm from $b=0.5$ fm to $b=2R_T$, where R_T denotes the target radius. Each parallel run here corresponds to a single Au+Au collision event. In central Au+Au collisions we have ~900 binary hard collisions at $\sqrt{s}=17.3$ GeV (cf. Fig. 8 of [56]) and ~1300 at $\sqrt{s}=200$ GeV. In every binary collision we produce one particle for each species (i.e., $J/\psi, \chi_c, \psi', D, \bar{D}, D^*, \bar{D}^*, D_s, \bar{D}_s, D_s^*, \bar{D}_s^*$), but with a different weight. Thus, for 20 parallel runs we get about 1.8×10^4 (or 2.6×10^4) perturbative particles for each species.

For each single parallel run at fixed b we obtain the final particle multiplicity for all particle species as well as integral quantities such as the transverse energy E_T as a function of rapidity y, the number of participants etc. Since we perform 20 parallel runs simultaneously, the spread in the distributions of particle multiplicities (or transverse energy) with respect to the individual runs provides some information on the fluctuations of particle multiplicities (as well as integral quantities). Vice versa, gating on events with fixed transverse energy E_T (in an interval $[E_T-\Delta E_T/2, E_T+\Delta E_T/2]$) from all impact parameter b we obtain a distribution in the impact parameter b that reflects the variation in centrality for the selected event class. However, for the observables presented

in Sec. III we have checked that the fluctuations in centrality have a minor impact on the normalized particle yields or ratios.

The statistics is sufficiently good to reach an accuracy of particle yields of a few percent in central collisions. This accuracy becomes worth for peripheral collisions. Here we increase the number of parallel runs in order to obtain approximately the same number of charmonia and open charm mesons for fixed impact parameter as for central collisions. Note, however, that the statistics also becomes worth when including experimental acceptance cuts at SPS or RHIC energies. Thus, when comparing to data, the overall accuracy is only on the ±5–7% level. This is also due to the fact that only some fraction of the initial charmonia survive the dynamical evolution due to a large number of dissociation reactions (see below).

III. RESULTS FOR NUCLEUS-NUCLEUS COLLISIONS AT SPS AND RHIC

A. SPS energies

Let us compare the charmonium suppression at SPS energies with experimental data from the NA50 Collaboration. This collaboration presents its results on J/ψ suppression as the ratio of the dimuon decay of J/ψ's relative to the Drell-Yan background in the 2.9–4.5 GeV invariant mass bin as a function of the transverse energy E_T, i.e.,

$$B_{\mu\mu}\sigma(J/\psi)/\sigma(DY)|_{2.9-4.5}, \tag{23}$$

where $B_{\mu\mu}$ is the branching ratio for $J/\psi \to \mu^+\mu^-$.

In the theoretical approaches we calculate the J/ψ survival probability $S_{J/\psi}$ defined as

$$S_{J/\psi} = \frac{N_{fin}^{J/\psi}}{N_{BB}^{J/\psi}}, \tag{24}$$

where $N_{fin}^{J/\psi}$ and $N_{BB}^{J/\psi}$ denote the final number of J/ψ mesons and the number of J/ψ's produced initially by BB reactions, respectively. In order to compare our calculated results to experimental data we need an extra input, i.e., the normalization factor $B_{\mu\mu}\sigma_{NN}(J/\psi)/\sigma_{NN}(DY)$, which defines the J/ψ over Drell-Yan ratio for elementary nucleon-nucleon collisions. We choose $B_{\mu\mu}\sigma_{NN}(J/\psi)/\sigma_{NN}(DY)=53$, in line with a recent NA50 compilation [47] obtained from experiments on proton collisions with lighter targets (cf. Sec. II A).

The experimental ψ' suppression is presented by the ratio

$$\frac{B_{\mu\mu}(\psi' \to \mu\mu)\sigma(\psi')}{B_{\mu\mu}(J/\psi \to \mu\mu)\sigma(J/\psi)}. \tag{25}$$

In our calculations we adopt this ratio to be 0.0165 for nucleon-nucleon collisions, which is again based on the average over pp, pd, pA reactions [47].

Figure 1 shows the ratio $B_{\mu\mu}\sigma(J/\psi)/\sigma(DY)$ as a function of the transverse energy E_T for S+U collisions at 200A GeV (upper part) and Pb+Pb collisions at 160A GeV (lower part). The solid line gives the HSD result within the comover absorption scenario for the cross sections defined by (18) while the various data points have been taken from Refs. [10,12,13]. The dash-dotted lines show results for the comover absorption scenario while the short dashed lines stand for the threshold suppression model (cf. Sec. II A). It is seen that all models are compatible with the data for S+U as well as Pb+Pb, which is essentially due to the fit of the matrix elements $|M_i|^2$ in Eq. (6) for the transport approach, $\sigma_{co}=1.0$ mb for the comover model, and the threshold participant densities $n_\chi=2.0$ fm^{-2} and $n_{J/\psi}=3.8$ fm^{-2} in the threshold suppression model. The statistical coalescence model (long-dashed line in the lower part of Fig. 1) also demonstrates a good agreement with the data for (semi)central ($N_{part}>100$ to 150) Pb+Pb collisions (the S+U data are outside its domain of applicability) due to a fit of the free parameters $\sigma_{c\bar{c}}^{NN}$ and $\xi_{\Delta y}$.

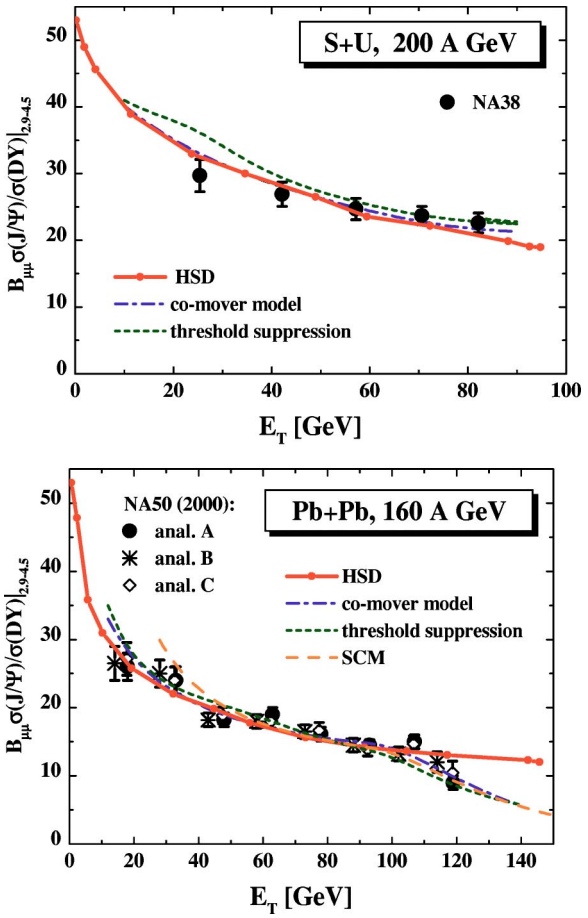

FIG. 1. (Color online) The ratio $B_{\mu\mu}\sigma(J/\psi)/\sigma(DY)$ as a function of the transverse energy E_T for S+U collisions at 200A GeV (upper part) and Pb+Pb collisions at 160A GeV (lower part). The solid lines with the full squares indicate the HSD results, the dash-dotted and short-dashed lines show the result of the suppression-only scenario (comover and threshold model, respectively), while the long-dashed line stands for the statistical coalescence model (SCM). The experimental data have been taken from Refs. [10,12,13].

For the proper description of the drop of the ratio (23) in Pb+Pb collisions at $E_T \approx 100$ GeV one has to take into account fluctuations of the transverse energy [46,69] and energy losses in the dimuon event sample [34,70]. To reproduce these effects in the transport approach, one would need

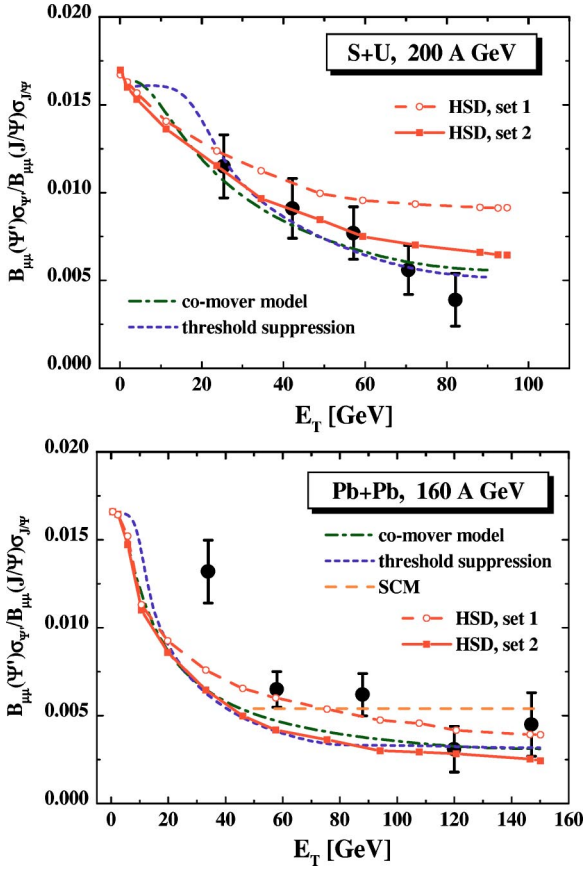

FIG. 2. (Color online) The ratio (25) versus the transverse energy E_T for S+U collisions at 200*A* GeV (upper part) and Pb+Pb collisions at 160*A* GeV (lower part). The dashed lines with the open circles and the solid lines with the full squares correspond to the HSD results calculated for two sets of parameters for the ψ' matrix element—set 1 and set 2 (21). The assignment of the other lines is the same as in Fig. 1. The experimental data have been taken from Refs. [13,71].

much better statistics, which is not feasible at present.

The $\psi'/J/\psi$ ratio (25) is shown in Fig. 2 versus the transverse energy E_T for S+U collisions at 200*A* GeV (upper part) and Pb+Pb collisions at 160*A* GeV (lower part) in comparison to the data from Refs. [13,71]. The dashed lines with the open circles and the solid lines with the full squares correspond to the HSD results calculated for two sets of parameters for the ψ' matrix element—set 1 and set 2 (21). Here the results for "set 1" overestimate the ratio for S+U at high E_T, whereas they are compatible with the ratio for Pb+Pb for $E_T \geqslant 60$ GeV. The calculations for "set 2"—including a larger matrix element for ψ'—systematically lead to a lower $\psi'/J/\psi$ ratio as a function of centrality. We note that no self energies for the $D,\bar{D}$ mesons have been incorporated so far. The latter change with baryon density and temperature and differ for D and $\bar{D}$ mesons [72]. As pointed out in Ref. [73] dropping $D,\bar{D}$ masses lead to an increase of J/ψ absorption by mesons and to a net lowering of the $\psi'/J/\psi$ ratio for central collisions.

The dash-dotted lines in Fig. 2 show the results for the comover absorption scenario, the short dashed lines stand for the threshold suppression model, while the long-dashed (constant) line indicates the SCM results for Pb+Pb. None of the models, however, reproduces the ratio for $E_T \approx 35$ GeV (for Pb+Pb). All approaches roughly yield a constant $\psi'/J/\psi$ ratio for Pb+Pb as a function of centrality for $E_T \geqslant 60$ GeV.

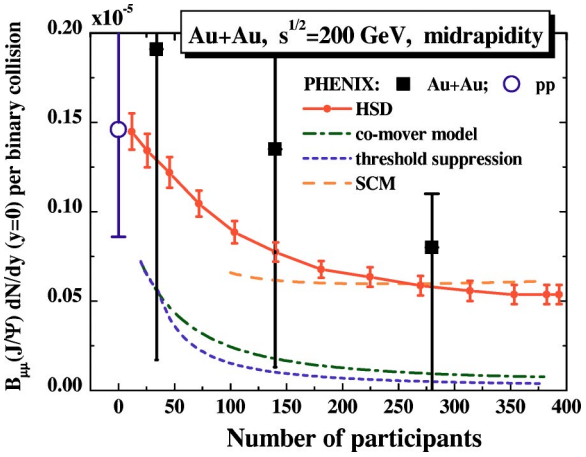

FIG. 3. (Color online) The calculated J/ψ multiplicity per binary collision—multiplied by the branching to dileptons—as a function of the number of participating nucleons N_{part} in comparison to the data from the PHENIX Collaboration [50] for Au+Au and *pp* reactions at $\sqrt{s}=200$ GeV. The assignment of the lines is the same as in Fig. 1.

B. RHIC energies

Whereas the differences between the results of the models are rather moderate at SPS energies due to a fit of the model parameters to the available data, the situation changes substantially at RHIC energies of $\sqrt{s}=200$ GeV. In Fig. 3 we show the calculated J/ψ multiplicity per binary collision—multiplied by the branching to dileptons—as a function of the number of participating nucleons N_{part} in comparison to the data from the PHENIX Collaboration [50] for Au+Au and *pp* reactions at $\sqrt{s}=200$ GeV. The solid line with the full circles indicates the HSD results, which roughly agree with the SCM results (long-dashed line) for $N_{part} \geqslant 100$. The dash-dotted line shows the results for the comover absorption scenario while the short-dashed line stands for the threshold model (with the parameters fixed at the SPS). It is seen that the comover absorption model as well as the threshold suppression model lead to an almost complete suppression of J/ψ in central collisions (cf. also Ref. [56]). As argued in Ref. [36] this large suppression in the comover model is essentially due to a neglect of the backward channels $D+\bar{D} \rightarrow$ charmonia+meson. In fact, the HSD calculations—that include the various backward channels—lead only to a moderate J/ψ suppression roughly compatible with the result of the SCM. This finding might suggest that the J/ψ and open charm degrees of freedom reach approximate chemical equilibrium for mid-central and central Au+Au collisions at the RHIC (see below). Unfortunately, the present data from PHENIX do not allow us to exclude any of the models so far.

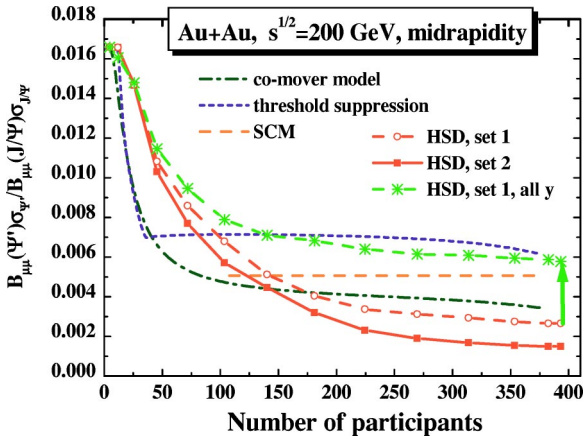

FIG. 4. (Color online) The midrapidity ratio (25) for Au+Au collisions at $\sqrt{s}=200$ GeV. The dashed lines with the open circles and the solid lines with the full squares correspond to the HSD results for two sets of parameters for the ψ' matrix element—set 1 and set 2 (21). The assignment of the lines is the same as in the previous figures. In addition, the line with crosses displays the rapidity integrated ratio (25) from HSD for set 1, which is even slightly above the SCM result for central collisions.

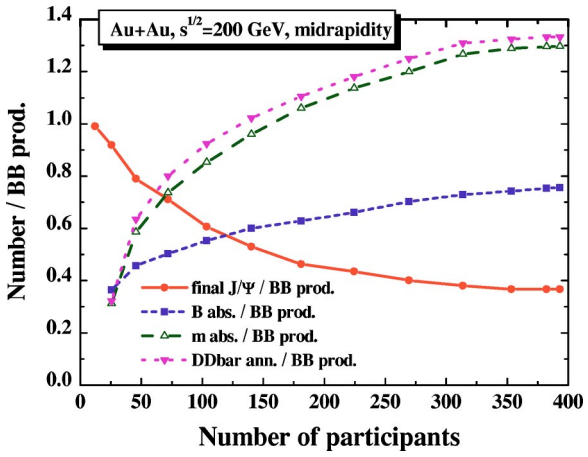

FIG. 5. (Color online) J/ψ absorption and recreation by $D\bar{D}$ annihilation versus N_{part} for Au+Au collisions at midrapidity at $\sqrt{s}=200$ GeV. The solid line with full circles shows the J/ψ survival probability (24), i.e., the number of final J/ψ mesons over the numbers of J/ψ initially produced by BB reactions (denoted as "BB prod."). Note: in all cases here the J/ψ numbers include the J/ψ from the decays of χ_c and ψ'. The dashed line with full squares shows the integrated rate of J/ψ absorption by baryons (26) over "BB prod.". The dashed line with open triangles stands for the rate of J/ψ absorption by mesons (27) (normalized again to the primary "BB prod.") and the dotted line with full triangles shows the integrated rate of J/ψ recreated by $D\bar{D}$ annihilations (28) (normalized to "BB prod.").

The $\psi'/J/\psi$ ratio (25) at midrapidity provides further information. It is displayed in Fig. 4 for Au+Au collisions at $\sqrt{s}=200$ GeV versus the number of participants N_{part}. The dashed lines with the open circles and the solid lines with the full squares correspond to the HSD results for two sets of parameters for the ψ' matrix element—set 1 and set 2 (21). These calculations give the lowest $\psi'/J/\psi$ ratio much below the ratio from the SCM (long-dashed line). The geometrical comover model (dash-dotted line) gives a higher ratio for central collisions than HSD. We attribute this difference to the fact that in the geometrical comover model only a single effective cross section appears for all charmonia independent of threshold effects for individual channels. The threshold model (short dashed line) provides the largest $\psi'/J/\psi$ ratio for central collisions even above the SCM results. Since the predictions of the models differ by factors up to four future experiments with high statistics should allow to exclude at least some of them.

In addition, we present in Fig. 4 (by the line with crosses) the rapidity integrated ratio (25) from HSD for set 1, which is slightly above the SCM result for central collisions, but still below the threshold model. This finding clearly demonstrates that midrapidity and rapidity integrated ratios have to be considered simultaneously before conclusions on the amount of chemical equilibration can be drawn.

C. Quantitative analysis of reactions rates from HSD

Whereas the results of the HSD transport approach for J/ψ show a rough agreement with the predictions from the statistical coalescence model for J/ψ (cf. Fig. 3), the ψ' to J/ψ ratios differ considerably at midrapidity (cf. Fig. 4). This demonstrates that a full chemical equilibrium might not be achieved in the transport calculations since the total number of c, $\bar{c}$ quarks are about the same in both models. In order to understand these differences in more detail it is of interest to have a closer look at the reaction rates from the HSD approach in total and in a differential way with respect to rapidity.

With this aim we show in Fig. 5 the J/ψ absorption and recreation by $D\bar{D}$ annihilation versus the number of participants N_{part} for Au+Au collisions at midrapidity for $\sqrt{s}=200$ GeV. The solid line with full circles, furthermore, shows the J/ψ survival probability (24), i.e., the number of final J/ψ mesons over the numbers of J/ψ initially produced by BB reactions (denoted as "BB prod."). We mention that the J/ψ numbers here include the J/ψ from the decays of χ_c and ψ'. The dashed line with full squares shows the integrated rate of J/ψ absorption by baryons

$$\int_{-\infty}^{\infty} dt \, \frac{dN_{J/\psi+B\to X}}{dt} \tag{26}$$

over the primary "BB prod.". As seen from Fig. 5 the final J/ψ is dominated by the dissociation with baryons. The dashed line with open triangles indicates the integrated rate of J/ψ absorption by mesons

$$\int_{-\infty}^{\infty} dt \, \frac{dN_{J/\psi+m\to D+\bar{D}}}{dt} \tag{27}$$

(normalized again to the primary "BB prod.") which is slightly lower than the dotted line with full triangles, which

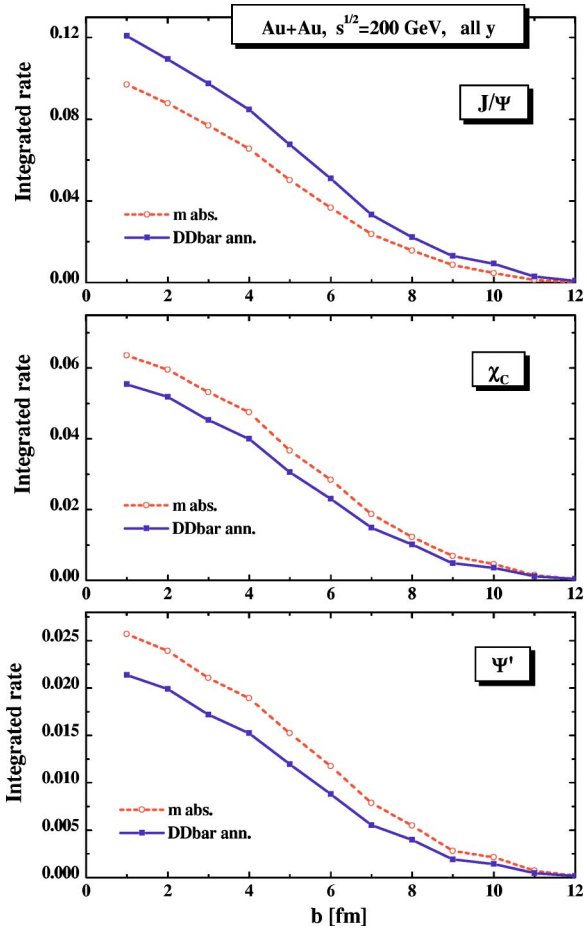

FIG. 6. (Color online) Integrated rate of J/ψ (upper part), χ_c (middle part), and ψ' (lower part) absorption by mesons (dashed lines with open circles) in comparison to the recreation by $D\bar{D}$ annihilation (solid line with full squares) as a function of the impact parameter b for Au+Au at $\sqrt{s}=200$ GeV.

stands for the integrated rate of J/ψ that are recreated by $D\bar{D}$ annihilations

$$\int_{-\infty}^{\infty} dt \, \frac{dN_{D+\bar{D}\to J/\psi+m}}{dt} \tag{28}$$

(normalized again to "*BB* prod."). Thus at practically all centralities—except for very peripheral collisions—the backward reactions by $D+\bar{D}$ annihilation overcompensate the "comover" meson absorption. Nevertheless, both integrated rates are approximately comparable suggesting an approximate dynamical equilibrium between charmonia, light mesons, and open charm mesons (cf. Ref. [36]). However, a full chemical equlibrium is not achieved in the transport calculations since the ψ' to J/ψ ratio still depends on the matrix element for the charmonium+meson coupling as seen explicitly by comparing the results from set 1 with those from set 2.

The question remains why the $\psi'/J/\psi$ ratios at midrapidity differ significantly in comparison to the SCM. To shed some light on this issue we show in Fig. 6 the time integrated rate of J/ψ (upper part), χ_c (middle part), and ψ' (lower part) absorption by mesons (dashed lines with open circles) in comparison with the recreation by $D\bar{D}$ annihilation (solid line with full squares) as a function of the impact parameter b. As already seen from Fig. 5 the J/ψ recreation by $D+\bar{D}$ annihilation is larger than the J/ψ dissociation with mesons. This situation is inverse for the χ_c (middle part) and ψ' (lower part) and essentially related to the higher mass of χ_c and ψ' which lead to substantially larger dissociation with pions due to the vicinity of the $D+\bar{D}$ threshold. On the other hand the backward channels for χ_c and ψ'+meson recreation are suppressed by phase space relative to the channel J/ψ +meson. One note of caution has to be added additionally: Due to sizable differences in cross section the χ_c and ψ' dissociation extends to much larger times than the backward recreation channels. Thus dynamically there is no common freeze-out; the higher mass charmonium states (χ_c and ψ') decouple at later times than J/ψ and may only be absorbed at late times but no longer recreated (see below).

Some further information on this issue is displayed in Fig. 7 where the rapidity distribution of the individual channels is shown for J/ψ (upper part) and ψ' (lower part). Though all production and absorption channels are rather flat in rapidity for $-2\leqslant y\leqslant 2$ the final J/ψ rapidity distribution (thick solid line) shows a local minimum for $-1\leqslant y\leqslant 1$. This effect—as a difference of large numbers—is related to the strong absorption with mesons and recreation by open charm and anticharm mesons. Thus the absorption of J/ψ mesons relative to the initial production by baryon-baryon collisions (full squares) shows a nontrivial rapidity dependence. These effects are even more pronounced for the ψ' (lower part) since the difference between the production and absorption channels is most effectively seen around midrapidity $-1\leqslant y\leqslant 1$, where the density of formed mesons is high and not very much delayed by formation time effects.

In addition we show in Fig. 8 the $\psi'/J/\psi$ ratio within the SCM as a function of the temperature T at freeze-out. The midrapidity ratios from HSD for set 1 and set 2 correspond to temperatures (in chemical equilibrium) of $\sim$150 and 130 MeV, respectively, whereas the SCM default result is displayed for $T=177$ MeV. Thus in HSD the dynamical freeze-out conditions especially for ψ' correspond to a later reaction phase than assumed in the SCM. This result is plausible in view of the large reaction cross sections for the channel $D+\bar{D}\leftrightarrow\psi'+$meson. Note, that the rapidity integrated ratio from HSD for set 1 corresponds to a temperature range from 175 to 190 MeV, which is significantly higher than at midrapidity. Consequently, one has to consider not only midrapidity ratios but their rapidity dependence as well to obtain firm conclusions on freeze-out conditions.

IV. SUMMARY

In summarizing this work we have found that (in absence of open charm enhancement in nucleus-nucleus collisions) the charmonium recreation by the backward $D+\bar{D}$ channels plays no substantial role at SPS energies, which leads to a good agreement between the comover and threshold suppres-

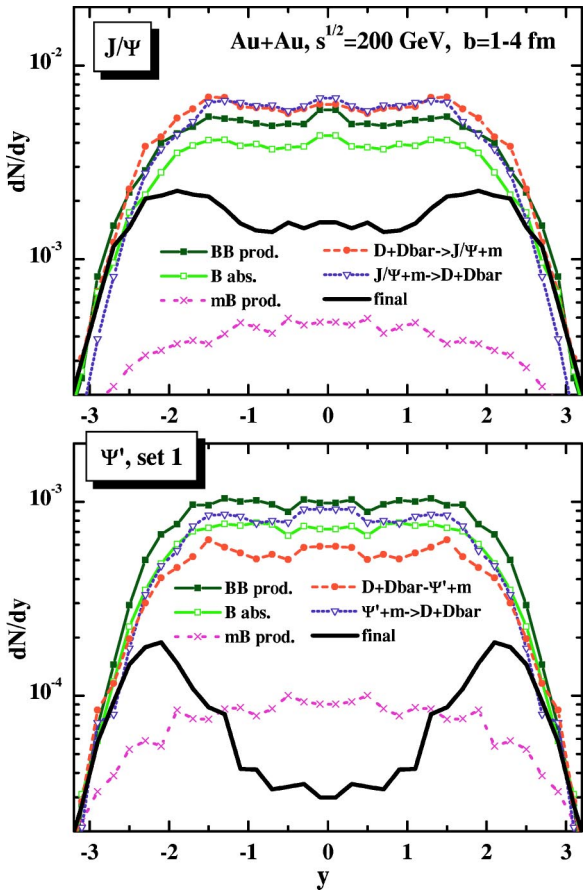

FIG. 7. (Color online) Rapidity distribution of J/ψ (upper part) and ψ' (calculated with set 1) production and absorption channels for central ($b=1-4$ fm) collisions of Au+Au at $\sqrt{s}=200$ GeV. The ordering of the different lines is as follows. The solid lines with full squares stand for the rapidity distribution of $J/\psi(\psi')$ mesons produced by initial BB collisions while the solid lines with open squares reflect the charmonia dissociation by baryons (B abs.); the dashed lines with crosses show the production by mB collisions. The dotted lines with open triangles show the $J/\psi(\psi')$ dissociation by mesons while the dashed lines with full circles stand for the recreation of charmonia by $D+\bar{D}$ annihilation. The full solid lines give the final J/ψ (upper part) and ψ' (lower part) rapidity distributions.

sion models and the HSD transport calculations at this energy. However, the backward $D+\bar{D}$ channels become substantial in Au+Au collisions at $\sqrt{s}=200$ Gev such that now an approximate agreement of HSD with the statistical coalescence model is achieved for the J/ψ in midcentral and central collisions. We point out that a full chemical equilibration for the hidden and open charm degrees of freedom is not achieved in the transport calculations on the basis of

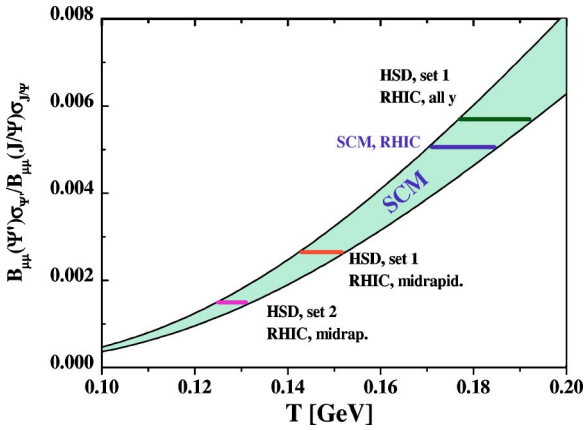

FIG. 8. (Color online) The ratio $\psi'/J/\psi$ within the SCM as a function of the temperature T. The upper and lower lines of the shaded area show the systematic uncertainty in the ratio that arises from uncertainties in the branching ratios. The results for the midrapidity ratios from HSD for set 1 and set 2 correspond to temperatures of ~150 and 130 MeV, whereas the SCM default result is quoted for $T=177$ MeV. Note that the rapidity integrated ratio from HSD for set 1 corresponds to a temperature range from 175 to 190 MeV.

hadronic interaction cross sections since the ψ' to J/ψ ratio still depends on the matrix element for the ψ' coupling to mesons. The latter statement is solid since the cross sections employed for the $J/\psi, \chi_c, \psi'+\text{meson} \leftrightarrow D+\bar{D}$ channels have to be considered as upper limits because they are obtained from a fit to the charmonium data from NA50 at SPS energies by discarding further absorption channels in a possibly prehadronic phase.

In addition we have provided predictions for the $\psi'/J/\psi$ ratio versus centrality, where the statistical coalescense model shows a larger value than the HSD approach at midrapidity. On the other hand, rapidity integrated ratios in HSD are slightly higher than the results from the SCM. This effect could be traced back to a significant rapidity dependence of the final ψ' yield, since the net ψ' absorption by mesons is maximal close to midrapidity. These pronounced differences can be exploited in future measurements at the RHIC to distinguish a hadronic rescattering scenario from quark coalescence close to the QGP phase boundary.

ACKNOWLEDGMENTS

The authors acknowledge inspiring discussions with P. Braun-Munzinger and A. Mishra. E.L.B. was supported by Deutsche Forschungsgemeinschaft (DFG) and GSI. A.P.K. was supported by DFG.

[1] H. Stöcker and W. Greiner, Phys. Rep. **137**, 277 (1986).
[2] W. Cassing and U. Mosel, Prog. Part. Nucl. Phys. **25**, 235 (1990).
[3] W. Cassing, E. L. Bratkovskaya, Phys. Rep. **308**, 65 (1999).
[4] *Quark Matter 2002* [Nucl. Phys. **A715**, 1 (2003)].
[5] *Strange Quark Matter 2003* [J. Phys. G **30**, 1 (2004)].
[6] T. Matsui and H. Satz, Phys. Lett. B **178**, 416 (1986).
[7] H. Satz, Rep. Prog. Phys. **63**, 1511 (2000).
[8] NA50 Collaboration, M. C. Abreu *et al.*, Phys. Lett. B **410**, 337 (1997).
[9] NA50 Collaboration, M. C. Abreu *et al.*, Phys. Lett. B **444**, 516 (1998).
[10] NA50 Collaboration, M. C. Abreu *et al.*, Phys. Lett. B **477**, 28 (2000).
[11] NA50 Collaboration, M. C. Abreu *et al.*, Phys. Lett. B **450**, 456 (1999).
[12] NA50 Collaboration, L. Ramello *et al.*, Nucl. Phys. **A715**, 243 (2003).
[13] NA38 Collaboration, M. C. Abreu *et al.*, Phys. Lett. B **449**, 128 (1999).
[14] N. Armesto and A. Capella, Phys. Lett. B **430**, 23 (1998); N. Armesto, A. Capella, and E. G. Ferreiro, Phys. Rev. C **59**, 395 (1999).
[15] R. Vogt, Phys. Rep. **310**, 197 (1999).
[16] C. Gerschel and J. Hüfner, Annu. Rev. Nucl. Part. Sci. **49**, 255 (1999).
[17] W. Cassing, E. L. Bratkovskaya, and S. Juchem, Nucl. Phys. **A674**, 249 (2000).
[18] D. E. Kahana and S. H. Kahana, Prog. Part. Nucl. Phys. **42**, 269 (1999).
[19] C. Spieles, R. Vogt, L. Gerland, S. A. Bass, M. Bleicher, H. Stöcker, and W. Greiner, J. Phys. G **25**, 2351 (1999); Phys. Rev. C **60**, 054901 (1999).
[20] L. Gerland, L. Frankfurt, M. Strikman, H. Stöcker, and W. Greiner, Nucl. Phys. **A663**, 1019 (2000).
[21] K. L. Haglin, Phys. Rev. C **61**, 031903 (2000); K. L. Haglin and C. Gale, *ibid.* **63**, 065201 (2001).
[22] Z. Lin and C. M. Ko, Phys. Rev. C **62**, 034903 (2000).
[23] Z. Lin, and C. M. Ko, J. Phys. G **27**, 617 (2001).
[24] A. Sibirtsev, K. Tsushima, and A. W. Thomas, Phys. Rev. C **63**, 044906 (2001); A. Sibirtsev, K. Tsushima, K. Saito, and A. W. Thomas, Phys. Lett. B **484**, 23 (2000).
[25] T. Barnes, E. S. Swanson, C.-Y. Wong, and X.-M. Xu, Phys. Rev. C **68**, 014903 (2003).
[26] B. Müller, Nucl. Phys. **A661**, 272c (1999).
[27] C. Y. Wong, E. S. Swanson, and T. Barnes, Phys. Rev. C **62**, 045201 (2000); **65**, 014903 (2002).
[28] F. O. Duraes, H. Kim, S. H. Lee, F. S. Navarra, and M. Nielsen, Phys. Rev. C **68**, 035208 (2003).
[29] B. Zhang, C. M. Ko, B.-A. Li, Z. Lin, and B.-H. Sa, Phys. Rev. C **62**, 054905 (2000).
[30] L. Grandchamp and R. Rapp, Phys. Lett. B **523**, 60 (2001); Nucl. Phys. **A709**, 415 (2002).
[31] P. Braun-Munzinger, and J. Stachel, Plasma Phys. **490**, 196 (2000); Nucl. Phys. **A690**, 119c (2001).
[32] M. I. Gorenstein, A. P. Kostyuk, H. Stöcker, and W. Greiner, Phys. Lett. B **509**, 277 (2001); J. Phys. G **27**, L47 (2001).
[33] A. P. Kostyuk, M. I. Gorenstein, H. Stöcker, and W. Greiner, Phys. Lett. B **531**, 195 (2002).
[34] A. P. Kostyuk, M. I. Gorenstein, H. Stöcker, and W. Greiner, J. Phys. G **28**, 2297 (2002).
[35] R. L. Thews, M. Schroedter, and J. Rafelski, Phys. Rev. C **63**, 054905 (2001).
[36] E. L. Bratkovskaya, W. Cassing, and H. Stöcker, Phys. Rev. C **67**, 054905 (2003).
[37] NA38 Collaboration, M. C. Abreu *et al.*, Eur. Phys. J. C **14**, 443 (2000).
[38] A. P. Kostyuk, M. I. Gorenstein, and W. Greiner, Phys. Lett. B **519**, 207 (2001).
[39] W. Cassing, L. A. Kondratyuk, G. I. Lykasov, and M. V. Rzjanin, Phys. Lett. B **540**, 1 (2001).
[40] J. P. Blaizot and J. Y. Ollitrault, Phys. Rev. Lett. **77**, 1703 (1996).
[41] D. Kharzeev, C. Lourenco, M. Nardi, and H. Satz, Z. Phys. C **74**, 307 (1997).
[42] NA50 Collaboration, P. Cortese *et al.*, Nucl. Phys. **A715**, 679 (2003).
[43] L. Gerland, L. Frankfurt, M. Strikman, H. Stöcker, and W. Greiner, Phys. Rev. Lett. **81**, 762 (1998).
[44] D. Kharzeev and M. Nardi, Phys. Lett. B **507**, 121 (2001).
[45] PHOBOS Collaboration, B. B. Back *et al.*, Phys. Rev. C **65**, 061901 (2002).
[46] J. P. Blaizot, P. M. Dinh, and J. Y. Ollitrault, Phys. Rev. Lett. **85**, 4012 (2000).
[47] NA50 Collaboration, B. Alessandro *et al.*, Phys. Lett. B **553**, 167 (2003)
[48] A. P. Kostyuk, M. I. Gorenstein, H. Stöcker, and W. Greiner, Phys. Rev. C **68**, 041902 (2003).
[49] M. Gaździcki, and M. I. Gorenstein, Phys. Rev. Lett. **83**, 4009 (1999).
[50] PHENIX Collaboration, S. S. Adler *et al.*, Phys. Rev. C **69**, 014901 (2004).
[51] A. Andronic *et al.*, Nucl. Phys. **A715**, 529 (2003); Phys. Lett. B **571**, 36 (2003).
[52] A. P. Kostyuk, hep-ph/0306123.
[53] P. Braun-Munzinger, K. Redlich, and J. Stachel, nucl-th/0304013.
[54] PHENIX Collaboration, K. Adcox *et al.*, Phys. Rev. Lett. **86**, 3500 (2001).
[55] PHENIX Collaboration, R. Averbeck, Nucl. Phys. **A715**, 695 (2003).
[56] W. Cassing, E. L. Bratkovskaya, and A. Sibirtsev, Nucl. Phys. **A691**, 753 (2001).
[57] PHENIX Collaboration, S. S. Adler *et al.*, Phys. Rev. Lett. **92**, 051802 (2004).
[58] E705 Collaboration, L. Antoniazzi *et al.*, Phys. Rev. Lett. **70**, 383 (1993).
[59] WA11 Collaboration, Y. Lemoigne *et al.*, Phys. Lett. **113B**, 509 (1982).
[60] Particle Data Group, K. Hagiwara *et al.*, Phys. Rev. D **66**, 010001 (2002).
[61] E672/E706 Collaboration, V. Abramov *et al.*, Report No. FERMILAB-Pub-91/62-E, IFVE-91-9, 1991.
[62] J. Geiss, W. Cassing, and C. Greiner, Nucl. Phys. **A644**, 107 (1998).
[63] D. Kharzeev, and R. L. Thews, Phys. Rev. C **60**, 041901 (1999).
[64] P. Braun-Munzinger, and K. Redlich, Eur. Phys. J. C **16**, 519 (2000); Nucl. Phys. **A661**, 546 (1999).
[65] K. Martins, D. Blaschke, and E. Quack, Phys. Rev. C **51**, 2723

(1995).
[66] J. Geiss, C. Greiner, E. L. Bratkovskaya, W. Cassing, and U. Mosel, Phys. Lett. B **447**, 31 (1999).
[67] W. Cassing and E. L. Bratkovskaya, Nucl. Phys. **A623**, 570 (1997).
[68] W. Cassing and C. M. Ko, Phys. Lett. B **396**, 39 (1997).
[69] A. Capella, E. G. Ferreiro, and A. B. Kaidalov, Phys. Rev. Lett. **85**, 2080 (2000).
[70] A. Capella, A. B. Kaidalov, and D. Sousa, Phys. Rev. C **65**, 054908 (2002).
[71] NA50 Collaboration, M. Gonin *et al.*, "Anomaly in charmonium in Pb+Pb collisions: Final results," Presented at 3rd International Conference on Physics and Astrophysics of Quark Gluon Plasma (ICPAQGP 97), Jaipur, India, 1997.
[72] A. Mishra, E. L. Bratkovskaya, J. Schaffner-Bielich, S. Schramm, and H. Stöcker, Phys. Rev. C **69**, 015202 (2004).
[73] L. Grandchamp, R. Rapp, and G. E. Brown, hep-ph/0306077.